Manuscript for K. Arimoto: Mechanism of Residual Stress Generation in Quenched Fe-Ni Alloy Cylinders Using Simulated Strains-Based Approach. HTM J. Heat Treatm. Mat. 78 (2023) (Posted on arimotech.net: Aug 2025)

Kyozo Arimoto 1,*

Mechanism of Residual Stress Generation in Quenched Fe-Ni Alloy Cylinders Using Simulated Strains-Based Approach

1 Doctor of Engineering, Arimotech Ltd., 4-3-2-701 Habucho, Kishiwada, Osaka 596-0825, Japan
* Corresponding author: kyozo_arimoto@arimotech.com

Abstract – To elucidate the mechanisms of residual stress generation in quenched steel parts has been a longstanding problem. Qualitative explanations for the changes in the stress distribution in quenched cylinders appeared in the 1930s when it became possible to measure residual stresses in specimens. The explanation at that time used the concept of thermal and transformation stresses, which is still included in current textbooks. This concept is referred to here as the estimated stresses-based approach. To simplify the explanation of stress generation due to the combined effects of temperature change and phase transformations, quenching experiments were devised using Fe-Ni alloys in which only martensitic transformation occurs. On the other hand, since heat treatment simulations provide strains resulting from thermal, phase transformation, plastic, transformation plastic, and creep phenomena, a method to elucidate the mechanism using these strains was devised in the early 2000s and named the simulated strains-based approach. This paper contrasts the estimated stresses-based and simulated strains-based approaches to the mechanism of residual stress generation in quenched Fe-Ni alloy cylinders and highlights the superiority of the latter.

Keywords: Residual stress, Sachs method, Fe-Ni Alloy, heat treatment simulation, and simulated strains-based approach

1. Introduction

Heat treatment simulation has been used to predict distortions and residual stresses in heat-treated steel parts. This provides information on various types of strain in treated parts, such as elastic, thermal, transformation, plastic, and transformation plastic strains. It was shown in the early 2000s that the mechanisms of heat treatment distortion and residual stress generation can be explained by examining the time variations of these various strain distributions, subsequently named the simulated strains-based approach [1].

The approach was also applied to the fundamental problem of the mechanism of residual stress development in the quenching of pure iron cylinders [1]. The results showed that this provides a clearer understanding of the occurrence of the phenomenon than the explanation using thermal stress by Rose [2], which has been used in textbooks for many years. Note that Rose extended his approach to quenched steel round bars in the next step, using the concept of transformation stress in addition to thermal stress. In this paper, the method of elucidating the mechanism of residual stress development using the concept of thermal and transformation stresses is called the estimated stresses-based approach.

To clarify Rose's explanation, the works of Bühler and Scheil [3], who first proposed the concepts of thermal and transformation stresses, are reviewed. They measured residual stresses in quenched cylinders of Fe-Ni alloys with different Ni contents to explain the combined effects of these two types of stresses. Based on the results, they qualitatively estimated how stress distributions occurred in a cross-section of cylinders with a specific Ni content.

For cylinders of this particular Ni content and similar process conditions, Rammerstorfer et al [4] carried out reproduction experiments. They measured residual stresses, which were used to validate their heat treatment simulation in its research phase. Based on these research results, Arimoto and Funatani [5] performed simulations for the same conditions, and applied the simulated strains-based approach to their results. This paper compares and discusses these results of applying estimated

stresses-based and simulated strains-based approaches.

2. Estimated stresses-based Approach

2.1. Rose's Explanation

Rose extended the approach to elucidate the mechanism of residual stress generation in the quenching of pure iron cylinders and applied it to water cooling of steel [2]. The development of the residual stress distribution in a 28 mm diameter 1.3 %C tool steel cylinder during water quenching was illustrated by drawing the schematic diagram in Figure 1a. The time-temperature-transformation diagram for continuous cooling of the tool steel cylinder is drawn at the top of the figure, where W indicates the point at which the temperature difference between the core and surface is at its maximum. In this tool steel cylinder, first, a pearlitic transformation occurs in the core, followed by a martensitic transformation in the periphery. The lower part of the figure shows the estimated stress changes on the surface and core of the cylinder and the measured residual stress distribution.

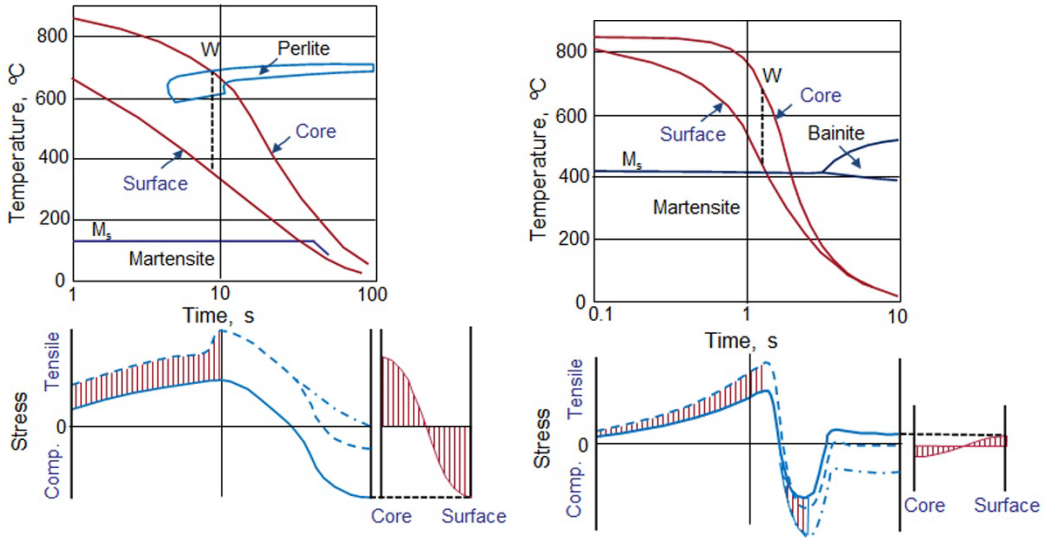

a) Shell-hardened cylinder b) Through-hardened cylinder

Fig. 1. Generation of residual stresses [2] in (a) Shell-hardened and (b) Through-hardened cylinders

As a similar example, the diagram for continuous cooling and stress evolution of a 10 mm diameter 22CrMo44 steel cylinder water quenched was depicted as shown in Figure 1b. The explanation given for this example is that the transformation of the entire part to martensite during quenching strongly counteracted the thermal stresses.

It is further explained that the stress variation in Figure 1 is qualitative, with the dashed line representing the stress assuming purely elastic behavior and the thick line on behalf of the stress after partial yielding corresponding to the temperature-dependent thermal yielding point. Note that thermal and transformation stresses are not drawn separately as lines.

2.2. Bühler et al.'s Explanation

Bühler et al. [6] reported in 1932 results of the Sachs method [7] for the measurement of residual stresses in the quenched steel cylinders. The method determines the triaxial component of residual stress along the radius from changes in length and outside diameter of a cylinder by successive drilling of its inner cross section. When this method was developed, it was reported that stresses up to several tens of MPa was reliably obtained [8].

They also attempted to explain the reasons for residual stress generations using the concepts of thermal and transformation stresses. As part of their results, they reported a schematic diagram of the change

in axial stress distribution in a quenched pure iron cylinder shown in Figure 2a [9]. The horizontal distribution state in the center of the lower part of Figure 2a occurs at the intersection point U where the core and surface stresses are zero. On the other hand, in the simulated results of this quenching experiment conducted by the author [1], as shown in Figure 1b, the intersection of stress changes at the core and surface occurs at a compressive stress state, and the stress distribution at that point is similar to the 8 s curve in Figure 2c.

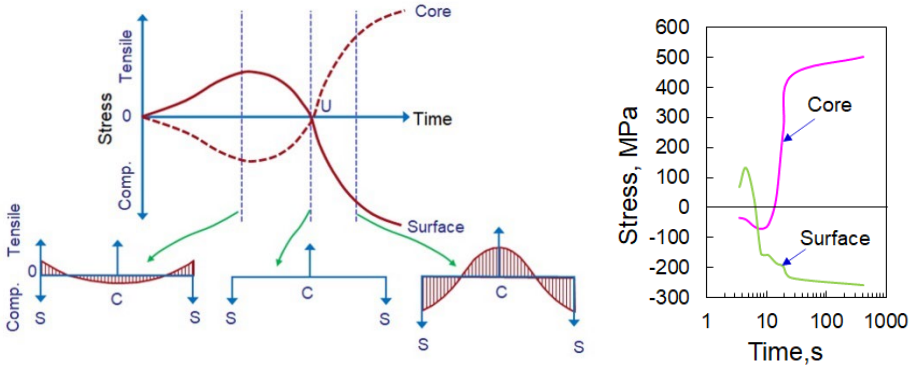

a) estimated at core and surface and along radius b) simulated at core and surface

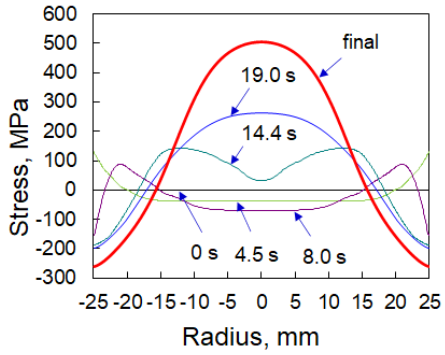

c) simulated along radius

Fig. 2. Temporal change of axial stress during rapid cooling of a pure iron cylinder; (a) estimated by Buchholtz and Bühler [9], (b) and (c) simulated by Arimoto [1].

To investigate the combined effects of thermal and transformation stresses, Bühler and Scheil [3] quenched cylinders (50 mm in diameter and 350 mm long) of Fe-Ni alloys with different Ni contents in water at 0 °C, and measured their residual stress distribution. Figure 3 shows only the axial component extracted from the original figure. They also obtained the relationship between Ni content and the start (Ms) and end (Mf) temperatures of martensitic transformation in Fe-Ni alloys as shown in Figure 4. Mf is below 0°C when Ni content exceeds 17 %. Diffusion-type transformations do not occur in the Fe-Ni alloys.

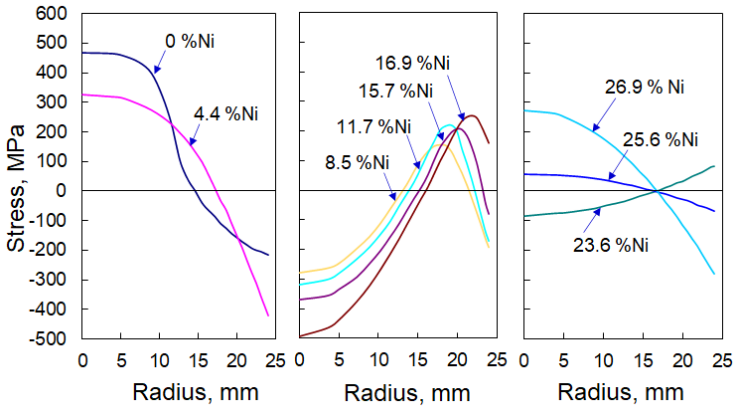

a) 0 - 4.4 %Ni b) 8.5 - 16.9 %Ni c) 23.6 - 26.9 %Ni

Fig. 3. Measured axial residual stress distribution in water quenched Fe-Ni alloy cylinders[3], (a) 0 - 4.4 %Ni, (b) 8.5 - 16.9 %Ni, (c) 23.6 - 26.9 %Ni

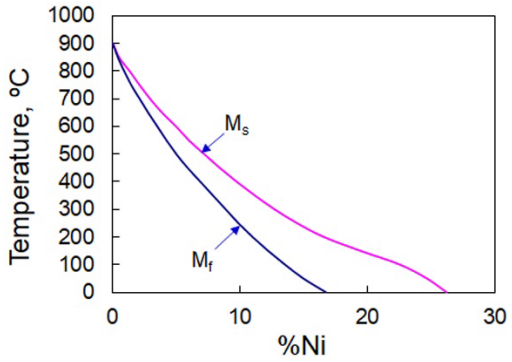

Fig. 4. Transformation start and end points of Fe-Ni alloys with different Ni contents during cooling [3]

Bühler and Scheil [3] drew the schematic diagram shown in Figure 5 for the changes in specific volume and stress during the quenching process of alloy cylinders with a Ni content in the range of 4.4 - 17 %. In the diagram, positions I, II, and III in the cross-section of the cylinder are shown. The stress distributions (a) and (b) in Figure 5 are estimated to occur at time Z1, when martensitic transformation begins, and at time Z2, when the transformation ends, at position I, respectively. The stress distribution (c) is approximated to occur at a point halfway between Z3, where position II starts the phase transformation, and Z4, where it ends. At position III, the core of the cylinder, the phase transformation starts at Z5 and ends at Z6. Stress distribution (d) is estimated at Z6. The distribution (e) resulting from the subsequent thermal contraction of the entire material corresponds to the measured residual stress.

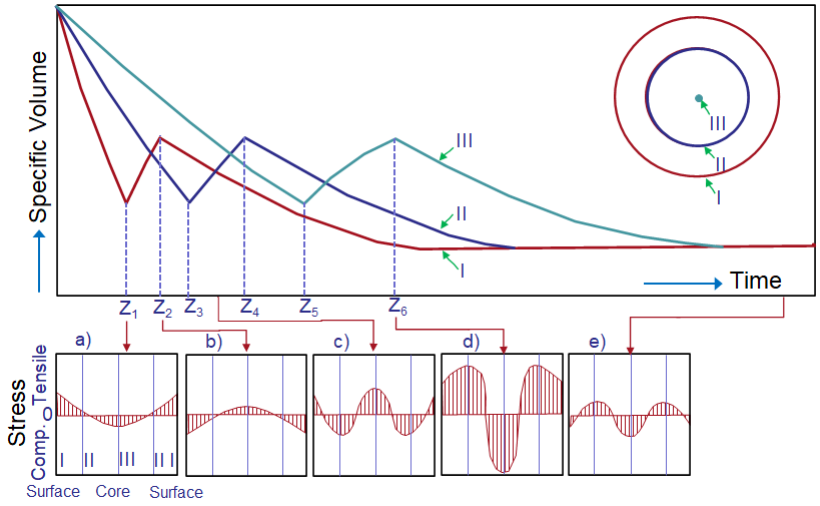

Fig. 5. Specific volume and stress changes in Fe-4.4-17 %Ni alloy cylinders (50 mm Dia.) during cooling [3]

On the other hand, experiments were carried out to investigate only the effect of transformation expansion on the residual stress distributions, using the property of Fe-Ni alloys that diffusion-type transformations do not occur [10]. Cylinders of 11.7 %Ni alloy were slowly cooled to 700 °C, 500 °C, or 360 °C, and then quenched in water at 0°C. The obtained axial residual stress distributions in the cylinders are shown in Figure 6 along with the curve for quenching from 900 °C.
During slow cooling of this alloy, no diffusion-type transformation occurs, and also plastic phenomena due to cooling shrinkage are minor. Therefore, only the effect of the next stage of water quenching can be compared in this experiment. The effect of cooling shrinkage has a significant influence on the residual stress if the starting temperature of water quenching is high. On the other hand, at lower temperatures, the effect of cooling shrinkage is reduced and the contribution of martensitic transformation becomes more pronounced. The above is reflected in the shape of the axial residual stress distribution in the cylinder shown in Figure 6.

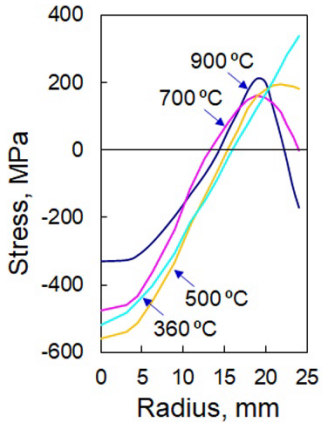

Fig. 6. Measured axial residual stress distribution in water quenched Fe-11.7%Ni alloy cylinders from specific temperatures [10]

2.3. Schulze et al.'s Explanation

Schulze et al. [11] reported a commentary on residual stress development due to heat treatment based on an estimated stresses-based approach in the early 1990s, after research works on heat treatment simulation had ended. It states that the aim is to study the development of thermal and transformation stresses during quenching separately and to discuss the residual stresses produced by each effect.

Schematic diagrams are given for a cylinder of ideal linear-elasticity, showing the individual changes in thermal and transformation stresses at the surface and core of the cylinder, and their superposition. Similar diagrams are produced for an elastoplastic cylinder; however, effects of transformation plasticity are not considered.

When the commentary by Schulze et al. was written, heat treatment simulation was available, even though it was still in the research phase. Therefore, it includes examples of simulation predictions for residual stress distributions caused by induction hardening of steel cylinders and laser hardening of steel plates. However, these examples do not describe thermal and transformation stresses and their combined effects.

3. Simulated Strains-Based Approach

3.1. Conditions of Simulations

Rammerstorfer et al [4] measured residual stresses in Fe-11.6 % Ni alloy cylindrical specimens (50 mm in diameter and 300 mm in length; quenched in water at 0 °C) using the Sachs method [7], as in the experiments of Bühler and Sheil [3]. The results of these measurements were then compared with their simulations. In the simulation of Rammerstorfer et al., modeling with 2D axisymmetric elements of the finite element method was performed for a short range in the longitudinal center of the specimen, based on the assumption of an infinitely long cylinder.

Rammerstorfer et al. measured material properties: thermal conductivity, specific heat, Young's modulus, Poisson's ratio, yield stress, work hardening factor, and coefficient of thermal expansion of the Fe-Ni alloy for their simulation. In their simulations, the effect of transformation expansion was handled by hypothetically including it in the coefficient of thermal expansion. The effect of transformation plasticity was addressed by reducing the yield stress in the range where phase transformation occurs. It is noted that a model based on the assumption that thermal strain and transformation strain are isotropic was used.

Simulations by Arimoto and Funatani [5] used the material property data from Rammerstorfer et al.'s, while the kinetics of martensitic transformation was modeled with the Koistinen-Marburger equation [12]. The transformation plastic strain rate was treated as being proportional to the rate of transformation and deviatoric stress. The FEM model of a cylinder with constraints was created in the same way as Rammerstorfer et al. In the heat transfer analysis model of Rammerstorfer et al. the cooling curve measured at the surface was directly specified as a boundary condition, and similar modeling was performed by Arimoto and Funatani. For the initial conditions of the analysis, Rammerstorfer et al. set an austenitic state at 900°C and assumed all strains and stresses to be zero at that stage, which was followed in the Arimoto and Funatani simulations.

3.2. Results from Simulations

The simulated temperature change at the core of the Fe-Ni alloy cylinder obtained by Arimoto and Funatani [5] is in good agreement with the experiment by Rammerstorfer et al. [4], as shown in Figure 7. Near the surface of the cylinder, the temperature reaches Ms immediately and martensite formation begins. On the other hand, martensite near the center begins to develop after 40 s. The measured surface temperature change in the figure was used as the boundary condition for the model.

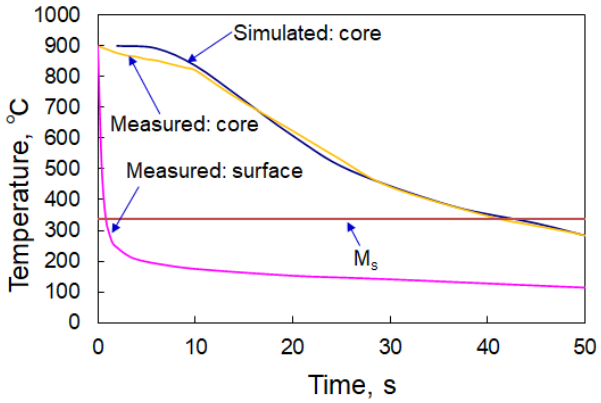

Fig. 7. Temperature changes in Fe-11.6 %Ni alloy cylinder [4,5]

The only phase transformation that occurs during the quenching of Fe-Ni alloys is martensitic transformation. Although the diagram of the simulation results for the progression of this phase transformation is not shown here, the phenomenon occurs at the surface of the cylinder after the temperature reaches Ms and progresses toward its core. The amount of transformation in the core gradually increases from around 36.4 s, and eventually, the entire cylinder transforms to martensite.

Figure 8 shows the distribution of the axial stress in the final cooling state simulated by Arimoto and Funatani, compared with the results measured by Bühler and Sheil, and Rammerstorfer et al. Stress distributions show compression in the core, tension around a radius of 15 to 20 mm, and compression at the surface. The result by Arimoto and Funatani is in generally agreement with the measurement of Rammerstorfer et al.

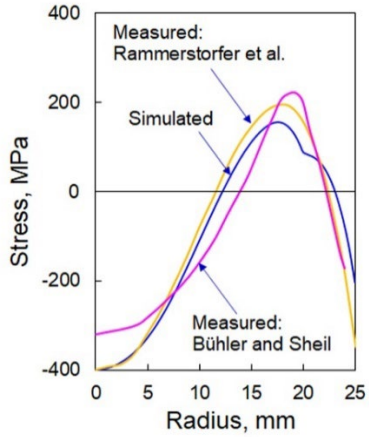

Fig. 8. Experimental and simulated axial residual stress in Fe-11.6 % Ni alloy cylinders [3,4,5]

Figure 9a shows the axial stress changes simulated by Arimoto and Funatani. Between time 2 s and 36.4 s, the stresses become compressive in the martensite formation zone. In contrast, the stress in the central austenitic zone is tensile, with a gradual increase in absolute value. After the core transforms to martensite, the absolute value of the tensile stress there decreases rapidly. Finally, the stress in the core becomes compressive.

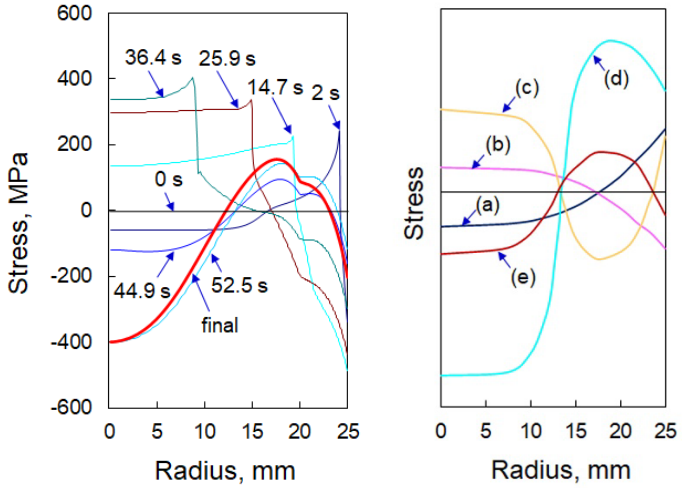

a) Simulated b) Estimated

Fig. 9. Axial stress changes in Fe-11.6 % Ni alloy cylinders obtained from (a) simulation [5] and (b) estimation [3]

Figure 9b shows the stress distributions qualitatively depicted by Bühler and Scheil in Figure 5, with the ratio on the vertical axis adjusted for comparison with Figure 9a. Apart from the presence of state (d) and the surface-side geometry of state (c), the trends of both distributions are consistent.

3.3. Explanation of Residual Stress Generation

What is described here are the results of Arimoto and Funatani's application of the simulated strains-based approach to the mechanism of residual stress generation in Fe-Ni alloy cylinders [5]. Since a linear relationship between elastic strain and stress can be used to elucidate stress development [1], the first focus is on understanding the mechanism of generation of the elastic strain distribution.

Changes in elastic strain are governed by an equilibrium equation that relates total strain to elastic, plastic, transformation, and transformation plastic strains [1]. Furthermore, the total strain in the longitudinal center of the cylinder is forced to be uniformly distributed over the cross-section by the infinite-cylinder assumption. The development of other strains depends on temperature, phase transformation, and stress conditions. Based on the above conditions, the process of elastic strain generation is clarified below.

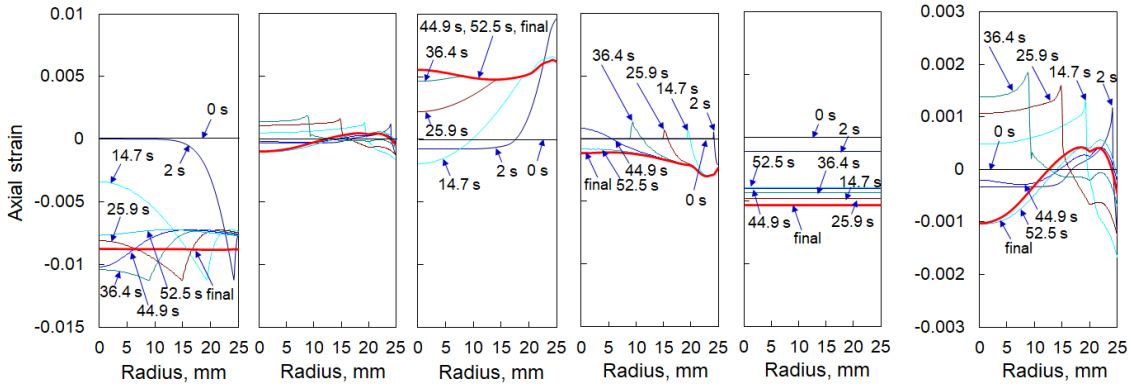

a) Expansion b) Elastic c) Plastic d) Trans. plastic e) Total f) Enlarged elastic strain

Fig. 10. Simulated axial (a) expansion, (b) elastic, (c) plastic, (d) trans. plastic (e) total, and (f) enlarged elastic strains change obtained for in Fe-11.6 %Ni alloy cylinder [5]

Figure 10 shows the time evolution of the axial components of the strains obtained from the simulation. Figure 10a included therein corresponds to the expansion strain, which is the sum of the thermal and transformation strains and is an isotropic quantity. As already mentioned, the expansion strain in the initial 900 °C austenitic state is assumed to have a uniform distribution of zero; the elastic, plastic, and transformation plastic strains shown in Figures 10b, 10c, and 10d, respectively, are also assumed to have zero distribution in the initial state. The total strain in Figure 10e is the sum of the four types of strain shown on its left side and is therefore initially zero-distributed.

As shown in Figure 10a, the thermal strain decreases from the surface side of the cylinder with the onset of cooling, and the negative area rapidly expands into the interior of the cylinder. On the other hand, in the range where martensitic transformation has occurred, the expansion strain returns to a positive direction due to the effect of the transformation expansion. The expansion strain in the final cooling state is uniformly distributed at -0.0088. On the other hand, the total strain is horizontally distributed at all stages, as shown in Figure 10e. As already mentioned, this is the case in the longitudinal center of a cylinder of sufficient length.

At 2 s in the initial cooling, the expansion strain decreases with thermal contraction on the surface side and recovers with its expansion in the range where martensitic transformation occurs, as shown in Figure 10a. On the other hand, the distribution of axial total strain is kept horizontal, so that the large drop in expansion strain is essentially compensated by the occurrence of positive elastic strain (Figure 10b) and plastic strain (Figure 10c) near the surface and the respective corresponding negative strains in the core. For the elastic strain, an enlarged scale on the vertical axis is shown in Figure 10f. In addition, negative transformation plastic strain occurs near the surface in the areas where martensitic transformation occurs, as shown in Figure 10d.

From 2 s onwards, the negative range of expansion strain near the surface extends towards the core, as shown in Figure 10a, and at 36.4 s this strain reaches its lowest level at the core. The positive elastic strain range progresses towards the core, as can be seen in Figure 10f, while the negative range on the surface side due to martensitic transformation extends inwards as well. The positive elastic strain in the core reaches its peak at 36.4 s. The behavior of this elastic strain distribution is similar to that of the axial stress component shown in Figure 9a.

The distribution of the plastic strain is shown in Figure 10c, where the positive area expands towards the core with time, and at 36.4 s there is a horizontal distribution of approximately 0.005, after which almost no change is observed. The transformation plastic strain, on the other hand, has a negative region that progresses towards the core, reaching a point with a radius of nearly 10 mm at 36.4 s, as shown in Figure 10d.

Between 36.4 and 44.9 s, the elastic strain shifts from positive to negative in the core and conversely from negative to positive near the surface, as shown in Figure 10f, and the shape of the distribution changes significantly. During this period, there is almost no change in the plastic strain, so the central increase in the expansion strain and the inward evolution of the transformation plastic strain produce such a significant change in the elastic strain distribution.

With the passage from 44.9 s to 52.5 s, the expansion strain further increases in the core due to the progress of transformation, and its distribution becomes almost horizontal at 52.5 s. The plastic strain hardly changes at this stage, and the transformation plastic strain decreases in the core. These effects lead to a decrease in elastic strain at the core, while the total strain distribution remains almost unchanged.

In the final cooling state, the expansion and total strains have horizontal distributions. It is therefore understood that the shape of the elastic strain distribution is determined by the difference between the distribution shape of the plastic and transformation plastic strains. On the other hand, a comparison of the axial elastic strain and stress distributions in Figure 10f and Figure 9a shows a similarity in the

shapes of the curves. This means that the mechanism of stress generation can be explained in the same way as that of elastic strain.

The simulation of Fe-Ni alloy cylinders described here did not yield the dimensional change of the cylinders due to quenching. However, this is possible if the heating process is taken into account. The axial and radial components of the total strain before and after quenching yield the changes in the length and diameter of the cylinder, respectively [1]. Therefore, the simulated strains-based approach has been applied to explain the mechanism of dimensional changes of cylinders, such as complete quenching of low-chromium steel cylinders, complete and incomplete quenching of carbon steel cylinders, and nitriding of steel cylinders [13].

4. Conclusions

This paper mainly compared the results of applying the estimated stresses-based approach and the simulated strains-based approach to the generation of quenched residual stress in Fe-Ni alloy cylinders. The former approach qualitatively estimates stress changes by referring to measured residual stress distributions, and thus it was not feasible to fully explain the details of the generation mechanism. The latter, on the other hand, logically explained the generation mechanism of residual stress distribution shapes by analyzing individual simulated strains and related results.

The simulated strains-based approach usually requires graphing the changes in individual strain distributions from the simulation results, as shown in this report. However, it is possible to determine which strains contribute significantly to the residual stresses and strains simply by analyzing the various strain distributions at the final cooling state. The actual problem solving is a matter of choosing the most effective procedure for the situation.

Heat treatment simulations are currently used simply as a substitute for experiments. As a result, only information on distortion and residual stresses is examined. However, a better understanding of the occurrence of these problems and the facilitation of their improvement can be achieved through the effective use of the strains obtained from simulation.

References

1. Arimoto, K.: Simulated Strains-Based Approach for Explaining Distortion and Residual Stress in Quenched Pure Iron Cylinder. Mater. Perform. Characterization, *11* (2022) 1, pp. 1–12, DOI: 10.1520/MPC20220027
2. Rose, A.: Eigenspannungen als Ergebnis von Wärmebehandlung und Umwandlungsverhalten. Härterei-Tecn. Mitt., *21* (1966) 1, pp. 1–6.
3. Bühler, H.; Scheil, E.: Zusammenwirken von Wärme– und Umwandlungsspannungen in abgeschreckten Stählen. Archiv. Eisenhüttenw, *6* (1933) 7, pp. 283–288.
4. Rammerstorfer, F. G.; Fischer, D. F.; Mitter, W.; Bathe, K. J.; M. D. Snyder: On Thermo –Elastic –Plastic Analysis of Heat–Treatment Processes Including Creep and Phase Changes. Computer & Structures, *13* (1981) 5-6, pp. 771–779.
5. Arimoto, K.; Funatani, K.: Historical Review of Residual Stress in Quenched Fe-Ni Alloy Cylinders and Explanation of Its Origin Using Computer Simulation. Proc. 24th Heat Treating Conference, ASM International, (2007), pp. 163–172.
6. Bühler, H.; Buchholtz, H.; Schulz, E. H.: Eigenspannungen bei der Wärmebehandlung von Stahl, Archiv. Eisenhüttenw. *5* (1932) 8, pp. 413–418.
7. Sachs, G.: Der Nachweis innerer Spannungen in Stangen und Rohren. Z. Metallkunde, *19* (1927) 9, pp. 352–357.
8. Sachs, G.: Praktische Metallkunde - Schmelzen und Gießen spanlose Formung, Wärmebehandlung, 1934, Verlag von Julius Springer.
9. Buchholtz, H.; Bühler, H.: Zusammenhang zwischen Wärmespannungen und Festigkeitseigenschaften von Stahl. Archiv. Eisenhüttenw. *6* (1933) 8, pp. 335–340.
10. Bühler, H., Scheil, E.: Einfluß der Abschreckbedingungen auf die Eigenspannungen von Stählen.

Archiv Eisenhüttenwes, 7 (1933) 6, pp. 359–363.
11. Schulze, V.; Vöhringer, O.; Macherauch, E.: Residual Stresses after Quenching – Quenching Theory and Technology, 2nd Edition, 2010, Imprint CRC Press.
12. Koistinen, D. P.; Marburger, R. E.: A General Equation Prescribing the Extent of the Austenite–Martensite Transformation in Pure Iron–Carbon Alloys and Plain Carbon Steels. Acta Met., *7* (1959) 1, pp. 59-60.
13. Arimoto, K.: A Brief Review on Validation for Heat Treatment Simulation, Proc. 31st ASM Heat Treat. Soc. Conf., (2021), pp. 71-80.